Materials Science & Engineering A 628 (2015) 423–432

Contents lists available at ScienceDirect

Materials Science & Engineering A

journal homepage: www.elsevier.com/locate/msea

Microstructure, texture and mechanical properties of cyclic expansion–extrusion deformed pure copper

N. Pardis [a,b], C. Chen [c,d], R. Ebrahimi [a,*], L.S. Toth [c,d], C.F. Gu [e], B. Beausir [c,d], L. Kommel [b]

[a] Department of Materials Science and Engineering, School of Engineering, Shiraz University, Shiraz, Iran
[b] Department of Materials Engineering, Tallinn University of Technology, Ehitajate tee 5, 19086 Tallinn, Estonia
[c] Laboratoire d'Etude des Microstructures et de Mécanique des Matériaux (LEM3), UMR 7239, CNRS/Université de Lorraine, F-57045 Metz, France
[d] Laboratory of Excellence on Design of Alloy Metals for low-mAss Structures (DAMAS), Université de Lorraine, France
[e] School of Aerospace, Mechanical and Manufacturing Engineering, RMIT University, Melbourne, VIC 3083, Australia

ARTICLE INFO

Article history:
Received 4 December 2014
Received in revised form
2 January 2015
Accepted 4 January 2015
Available online 9 January 2015

Keywords:
Severe plastic deformation
Cyclic expansion–extrusion
Copper
EBSD
Texture
Mechanical properties

ABSTRACT

A recently developed severe plastic deformation technique, cyclic expansion–extrusion (CEE), was applied on a commercial pure copper to investigate the relationship between microstructure, texture and mechanical properties over a wide range of strains. Microstructure and crystallographic texture investigations were performed by optical microscopy, electron back scattering and X-ray diffraction. Significant evolution in grain refinement was achieved down to sub-micron grain size. A considerable texture evolution was also observed within the deformation zone with the extrusion as the decisive step for the final texture. Fiber deformation textures were observed; the ⟨111⟩ component was found to be the main texture component while the ⟨100⟩ component became significant only at very large strains. The evolution in hardness and tensile properties was studied and a clear relationship between texture evolution, microstructural parameters and mechanical properties was found and discussed.

1. Introduction

Research in the field of severe plastic deformation (SPD) has been developing rapidly in the last decade. In this regard, considerable attention has been devoted to high pressure torsion (HPT) [1] as well as equal channel angular pressing (ECAP) [2–5] as the two best-known SPD techniques for producing ultrafine-grained (UFG) materials. Although these methods are powerful tools for processing UFG materials [6–11], other techniques are still worth considering as they have different advantages and can compete with HPT or ECAP for industrial applications [10–13].

Different from the conventional SPD techniques, cyclic expansion–extrusion (CEE) is a recently introduced SPD technique based on the direct extrusion process [14,15] and advantageous with respect to cyclic extrusion–compression (CEC) [16], by suppressing the need for applying external back pressure which is usually carried out by complicated systems [17–19]. It is also simpler than repetitive upsetting–extrusion (RUE), in which the exit channel is blocked to provide back pressure on the extruded material [20,21]. However, the deformation is not steady in these techniques which leads to inhomogeneous deformation and even folding of the processed material [22,23]. Such problems/limitations, however, do not exist in the CEE method and therefore, the CEE technique has good potential for SPD processing of materials. So far, limited investigations were conducted on this method [14,15] and detailed investigations are still needed for better understanding the characteristics of this new SPD technique. Therefore, this research is dedicated to CEE processing of copper samples to gain an insight into the process as well as into the structural–mechanical property relationship up to large accumulated strains.

2. Experimental

2.1. Material and processing

Commercially pure copper rod was machined to obtain samples with 10 mm diameter and 60 mm length; they were annealed for 2 h at 650 °C, and then furnace cooled to room temperature. This heat treatment led to an average grain size of about 10 μm which is an optimum grain size for characterizing the initial microstructure by EBSD and by X-ray, it also provides more homogeneous structure with respect to the specimen size. Before testing, the samples were covered with Teflon® tape and then extruded in a specially designed CEE die. During processing, the sample is first

* Corresponding author. Tel./fax: +98 711 2307293.
E-mail addresses: pardis@shirazu.ac.ir, npardis@gmail.com (N. Pardis), ebrahimy@shirazu.ac.ir (R. Ebrahimi), laszlo.toth@univ-lorraine.fr (L.S. Toth).

http://dx.doi.org/10.1016/j.msea.2015.01.003
0921-5093/

expanding in diameter from $D_0=10$ to $D_m=14.2$ mm in the expansion part of the die. Then, the expanded sample retrieves its initial geometry in the extrusion stage of the CEE process (Fig. 1a). Note that the two conical parts of the die are different; in order to ease the starting of the deformation process, the inlet cone has a smaller angle (Fig. 1a). The sequences of the CEE process are schematically shown in Fig. 1b–d. The process can be repeated several times by consecutive pressing of the samples. The process starts with a sacrificial sample to fill up the die by closing the output channel (Fig. 1b), then the exit is opened and the first main sample (sample 1) is put into the inlet channel (Fig. 1c). This sample becomes the first-pass sample. For removing this sample, a second one is used to push it out (Fig. 1d). Any desired number of samples could be involved in this sequence of pressings to obtain samples at different number of passes. In all cases, the back-pressure necessary for the deformation of a sample is provided by the preceding sample to be extruded, which is still in the die, filling it up to its inlet point. For several passes, successive pressing of the previously processed samples are performed in a cyclic manner, one is always pushing out the other (an example is shown in Fig. 1d). Up to 16 passes were achieved in this work and samples were processed for different number of passes. The extrusion was done at a constant ram speed of 0.2 mm/s, at room temperature using a screw driven pressing machine. This speed was chosen to be low enough to avoid any significant heating so that the deformation generated heat could be evacuated by the die structure and the test temperature could be maintained at room temperature.

2.2. Microstructure and texture measurements

For studying the structural evolution in the samples, they were cut parallel to the extrusion direction. The obtained surfaces were polished and subsequently etched with a mixture of 100 mL distilled water, 8 mL sulfuric acid, 2 g potassium dichromate and 1 drop hydrochloric acid per 25 mL of solution [24]. The resulting microstructure was studied by polarized optical microscopy and by electron back scatter diffraction (EBSD). Prior to investigations, the selected surface of each sample was electro-polished for 6 s at 268 K in an electrolytic solution of 33% HNO_3 and 67% methanol with a DC voltage of 13 V. EBSD investigations were performed by a JEOL 6500F scanning electron microscope (FEG-SEM) equipped with a field emission gun operating at 15 kV. Inverse pole figure (IPF) maps were prepared from the measurements using the EBSDMCF software package [25]. The pixel size in the EBSD measurements was 0.7 µm for the initial material, 0.4 µm for the 1-pass, 0.09 µm for the 4-pass and 0.07 µm for the samples deformed up to 8 and 16 passes. Grain boundaries were identified using 5° minimum disorientation angle between two adjacent pixels which led to the identification of the grains having continuous closed boundaries with at least 5° grain boundary angle. Grain orientations were then defined as the average of the pixel orientations constituting the grain and then disorientation angle between adjacent grains was obtained using these average values. This procedure leads to the next-neighbor disorientation distribution of the microstructure [26].

The crystallographic texture was measured by X-ray using CuKα radiation at a wavelength of 0.15406 nm. Three incomplete pole figures ({111}, {200}, {220}) were obtained up to 70° inclination angle from which the orientation distribution function (ODF) was calculated using the spherical harmonics technique. From the continuous ODF the complete pole figures were recalculated using the JTEX software [27].

2.3. Mechanical tests

Vickers microhardness measurements were performed by applying 50 g load at a loading rate of 5 g/s and 15 s dwell time on a polished section normal to the extrusion direction. Microhardness indentations were performed with an incremental distance of 0.5 mm along two diameters and the average value of 40 indentations was considered as the Vickers microhardness value of the sample. These measurements were conducted on the initial annealed sample as well as on the CEE processed samples after 1, 2, 4, 6, 8, 10, 12 and 16 CEE passes. In addition to the microhardness measurements, a Zwick universal hardness tester was used to trace indentation load–displacement values at different positions within the CEE deformation zone. Tensile test specimens with gage length and gage diameter of 10 mm and 8 mm, respectively, were machined along the CEE processed samples in the longitudinal direction. An Instron 8516 machine was used to perform tensile tests at room temperature, with a constant ram speed of 0.5 mm/min (initial strain rate: $8.3\times10^{-4}\,s^{-1}$).

3. Finite element analysis

The imposed strain can be considered as quantitative parameter measuring the amount of severe plastic deformation in SPD techniques. Pardis et al. [14] calculated the imposed strain value in CEE for ideal deformation conditions. However, the previous investigations on axisymmetric and non-axisymmetric versions of the CEE process [14,15] revealed that there exists some additional redundant shear deformation, like in other deformation techniques [28], which has to be considered in the strain calculation. In this regard, finite element method (FEM) was used to calculate a more accurate strain value per each CEE pass by evaluating the strain distribution. ABAQUS/explicit software was used for modeling the die, the sample and the punch in axisymmetric condition. The die geometry parameters used in the FEM simulations are shown in Fig. 1a.

The die and punch were considered as rigid bodies while the sample was defined to be deformable and was meshed with 4-node bilinear axisymmetric quadrilateral elements (CAX4R) [29]. The constitutive equation for the von Mises flow stress of the sample was defined by Eq. (1) which is a recommended constitutive equation for pure copper over a wide range of strains [30].

$$\sigma=27.12+356\left[1-\exp\left(\frac{-\varepsilon^{0.86}}{0.28}\right)\right]\ (\mathrm{MPa}) \tag{1}$$

Frictionless condition was considered at the die–sample interface which makes it possible to consider only the intrinsic redundant strain during the process and eliminating the effect of friction work [28] at the die–sample interface. The use of Teflon® as lubricant also ensures that the friction coefficient remains very small; about $\mu=0.02$, see in Ref. [12].

4. Results and discussion

4.1. Strain calculation

One can calculate an average von Mises strain from the geometric dimensions of the die using only the normal components of the strain tensor [14]

$$\overline{\varepsilon}=4\ln\left(\frac{D_m}{D_0}\right)=1.403 \tag{2}$$

However, as mentioned in Section 3 above, accurate strain evaluation also needs to take into account the redundant shear

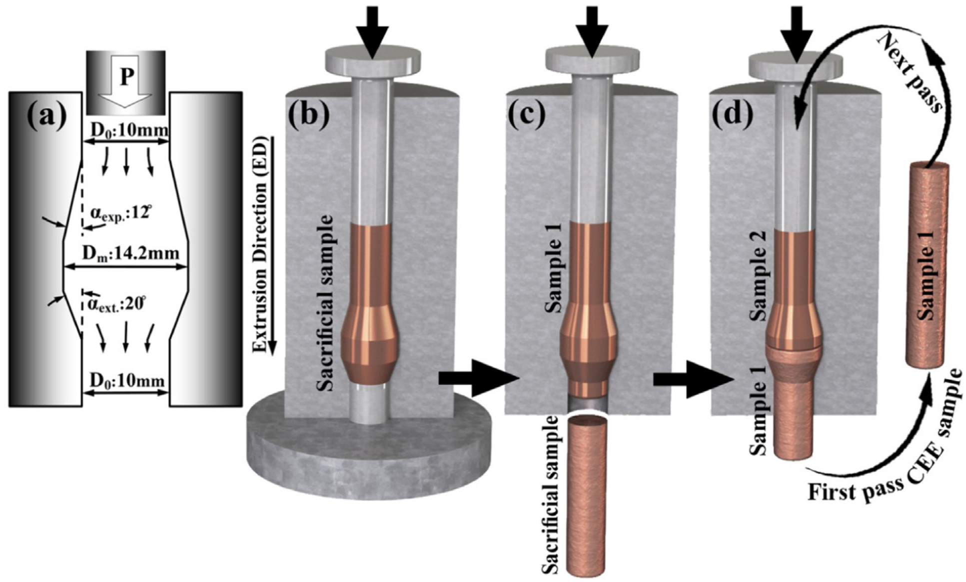

Fig. 1. Schematic illustration of the cyclic CEE process. (a) die dimensions, (b) expansion of the sacrificial sample with closed die, (c)–(d): the cyclic process with two samples.

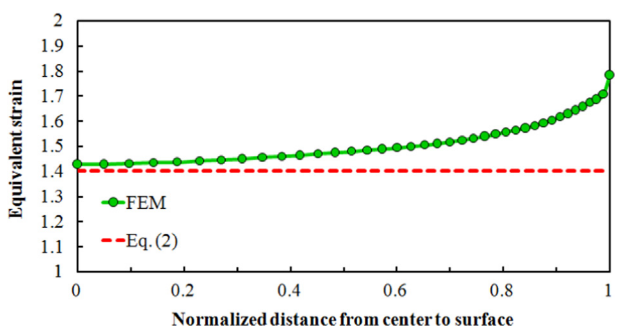

Fig. 2. Accumulated strain distribution along the radius of the sample after one CEE pass.

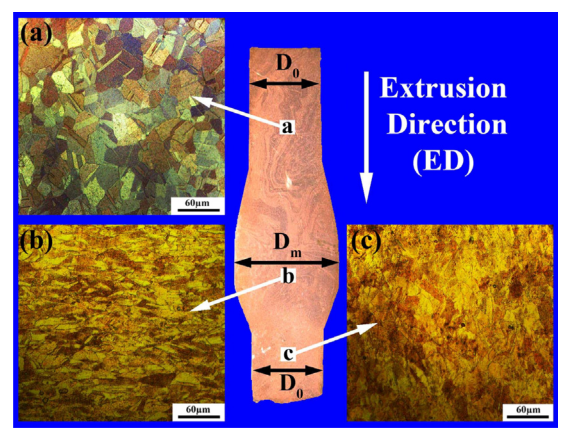

Fig. 3. In-situ configuration of a sample during the CEE process showing its microstructure in (a) undeformed, (b) expanded, (c) extruded states.

strain component, which is automatically considered in FEM. The accumulated strain along different strain paths was calculated by FEM as a function of the starting radius position in one CEE pass; the results are presented in Fig. 2. The strain value in the center position is very close to the strain value given by Eq. (2), then it gradually increases with the radius. As can be seen, the redundant shear is making significant contribution to the total strain near to the external radius (Fig. 2). Therefore, the average value of the strain distribution $\varepsilon_{av.} \cong 1.5$ was considered as the average strain value imposed to the sample in each CEE pass in this study (with the die geometry parameters given in Fig. 1a). Note that the location for EBSD analysis on the samples was taken at 2 mm from the surface where the strain value is very close to the considered average value of $\varepsilon_{av.} \cong 1.5$.

4.2. Optical microscopy

The results of the optical microscopy observations obtained on the longitudinal section of a one-pass deformed sample are shown in Fig. 3. As can be seen from the geometry of the deforming sample – obtained from an interrupted test – the sample completely filled the die chamber, so it is guaranteed that the strain was accumulated to its expected total value within the sample. The metallographic images obtained at three positions along the centerline are displayed in Fig. 3: undeformed material (a), middle of the deformation zone (b) and extruded part (c).

The initial annealed structure (Fig. 3a) gradually evolves into a pancake like structure in the expansion region (Fig. 3b) to satisfy the geometrical changes in the sample which represents a pure shear mode of deformation along the centreline. The average aspect ratio of the grains at this state was measured to be ~ 2.75, which is not far from the theoretical value of 2.86. By subsequent extrusion step, these expanded grains transform back into an equiaxed structure (Fig. 3c). However, the resulting microstructure is different from the initial one because of the large imparted strain (more detailed discussion on the microstructure using EBSD results are presented in Section 4.3 below).

4.3. EBSD analysis

A fully annealed grain microstructure is seen in the sample before CEE processing (Fig. 4) displaying a high fraction of annealing twins. The location for EBSD analysis on the sample is illustrated in Fig. 4c. The presence of the large number of twin boundaries leads to a high peak in the disorientation angle distribution (Fig. 4b) at 60°. Another peak is also seen at 40° which belongs to a coincident site lattice of CSL=9; it is also typical for recrystallization of Cu. The presence of these two peaks

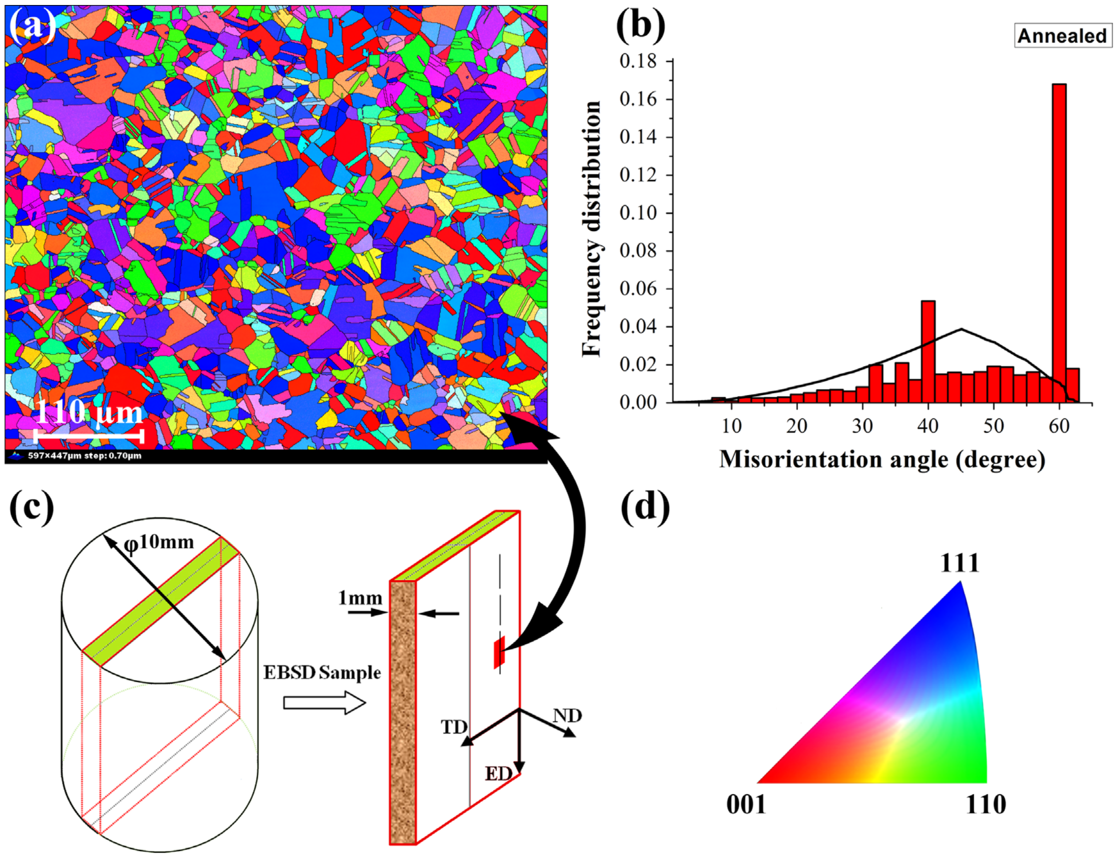

Fig. 4. (a) Inverse pole figure EBSD map of the annealed sample, (b) grain-to-grain misorientation distribution from the IPF map in comparison with the random Mackenzie distribution (solid line), (c) schematic illustration of the location of the EBSD measurement within the sample, and (d) the key color figure for the extrusion axis. (For interpretation of the references to color in this figure legend, the reader is referred to the web version of this article.)

makes the disorientation distribution very different from the random Mackenzie distribution [31,32] (Fig. 4b solid line).

In order to understand the evolution of the texture and the microstructure, we have studied in detail the first-pass sample by interrupting the test. The IPF-EBSD maps of the expanded and extruded materials within the first CEE pass (locations (b) and (c) in Fig. 3) are displayed in Fig. 5a and b, respectively. The EBSD-observed microstructures are similar to what was observed by optical microscopy (Fig. 3b and c). However, by considering the dominant color of grains in each IPF map (mostly green in Fig. 5a and blue and red in Fig. 5b) we observe a significant texture evolution within one CEE pass which will be discussed in more details in Section 4.5.

Comparison of Figs. 4b and 5c reveals an increase in the fraction of low angle boundaries. This increasing trend continues by further straining in the extrusion step by a sharp peak below 15° (Fig. 5d). After expansion during the first pass, the misorientation distribution is close to the random Mackenzie distribution. However, this distribution becomes very different after the subsequent extrusion stage because the fraction of low angle boundaries significantly increases from about 15% to more than 35% (Fig. 8).

It was observed that after the first pass the equiaxed shapes of the initial grains are nearly recovered (Figs. 3c and 5b) due to the inversion in the strain, because the expansion step is followed by the same amount of area reduction in the extrusion stage. However, significant structure changes took place within the grain interiors. This is illustrated in Fig. 6a showing the internal structure of two neighbor grains after the first pass. The initial grain boundary is depicted by arrows and a high density of low angle boundaries is seen within the grains. The average size for these sub-grains goes down to about 400 nm (Fig. 6a and b).

Fig. 7 presents the next neighbor misorientation angle distribution between neighbor grains as a function of CEE passes. It was previously shown that after the first CEE pass the frequency of low angle boundaries (with misorientation angles less than 15°) increases significantly (Fig. 5d) due to the grain fragmentation process (shown in Fig. 6). After the fourth pass, however, the major feature of the misorientation distributions is the presence of two peaks (Fig. 7a); one at small angles and one at large angle and there is not much evolution of the disorientation distribution after eight passes (Fig. 7b and c).

Fig. 8 simultaneously illustrates the evolution in low angle grain boundaries (LAGBs) and average misorientation angle during subsequent CEE passes. It is seen that the fraction of LAGBs increases during the first pass (after expansion and extrusion) and consequently, the average misorientation angle decreases. Further processing, however, decreases the fraction of LAGBs reaching a steady state condition at eight passes. At the same time the average misorientation angle increases to a steady state value which is still lower than its value in the annealed condition (due to the absence of twin boundaries). This increase indicates the evolution of the submicron size sub-grains (with low angle misorientation) into high angle boundaries. The decrease in the fraction of LAGBs between passes one and eight (Fig. 8) is due to a progressive slow-down of the grain fragmentation process which is believed to be due to a significant reduction in generation of geometrically necessary dislocations (GNDs) [6] ending up in a constant average grain size ~718 nm (in number-weighing) at extreme large strains (Fig. 9).

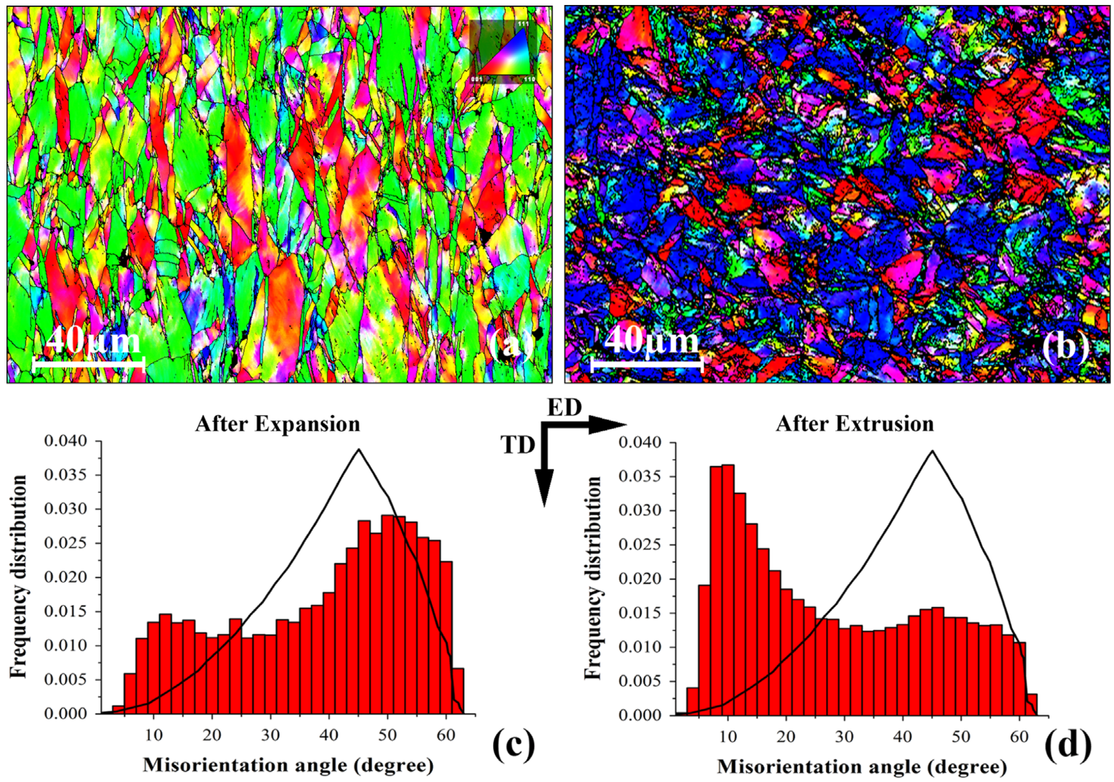

Fig. 5. Inverse pole figure EBSD maps during/after one CEE pass: (a) after expansion, (b) after extrusion; next-neighbor grain misorientation angle in comparison with the random Mackenzie distribution (solid line): (c) after expansion, (d) after extrusion.

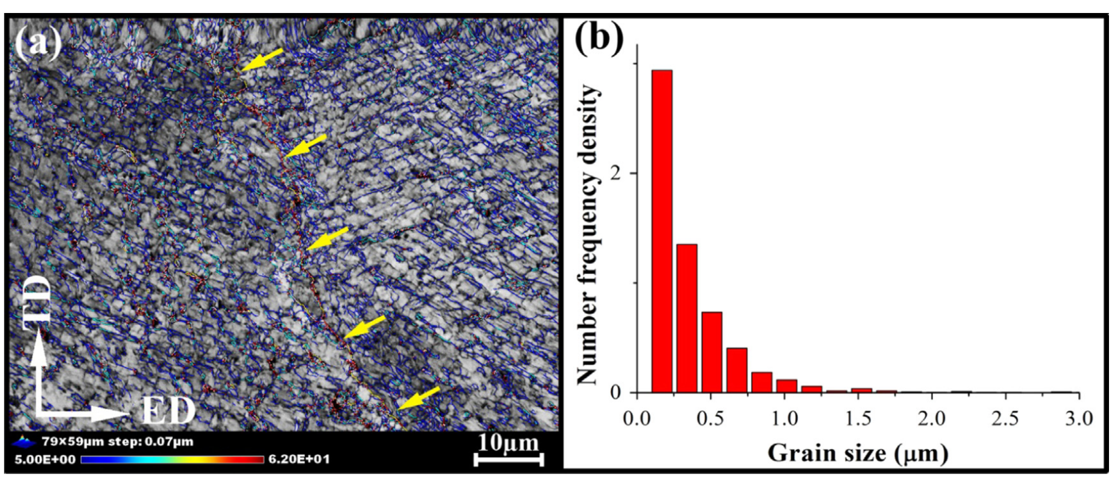

Fig. 6. Microstructure after one CEE pass showing the grain interior of two grains by EBSD: (a) superimposed band contrast and boundary map (for the angles in latter, use the color code displayed in the color bar), (b) number-weighed grain size distribution within the grains after the first pass (the grain boundary angle minimum is 5°). (For interpretation of the references to color in this figure legend, the reader is referred to the web version of this article.)

The variation of the average grain size as a function of pass-number/strain is displayed in Fig. 9 for both number and area-weighed calculations. As expected, the area-weighed values are always higher than the number-weighed ones. They are, however, quite near to each other for the initial and final states. This means that in these limiting states the grain size distribution must be relatively narrow (for equal values, both distributions should be nearly Dirac-delta functions). Important deviations, however, exist between the area and number-weighted average grain sizes in the initial stage of grain refinement, between the 1/2 and 4 passes. This means that in this stage there is a kind of 'duplex' structure due to the ongoing grain fragmentation process which produces many small grains mostly in the vicinity of the grain boundaries of the initial large grains while leaving relatively large regions of the grains not divided.

4.4. Mechanical properties

Indentation load–displacement curves were measured at three locations indicated by (a–c) in Fig. 3 and are displayed in Fig. 10. These curves clearly show that the final indentation depth decreases as the material passes through the deformation zone. The difference in indentation depth in the undeformed and expanded locations is much larger compared to the corresponding value for expansion and the subsequent extruded states. This

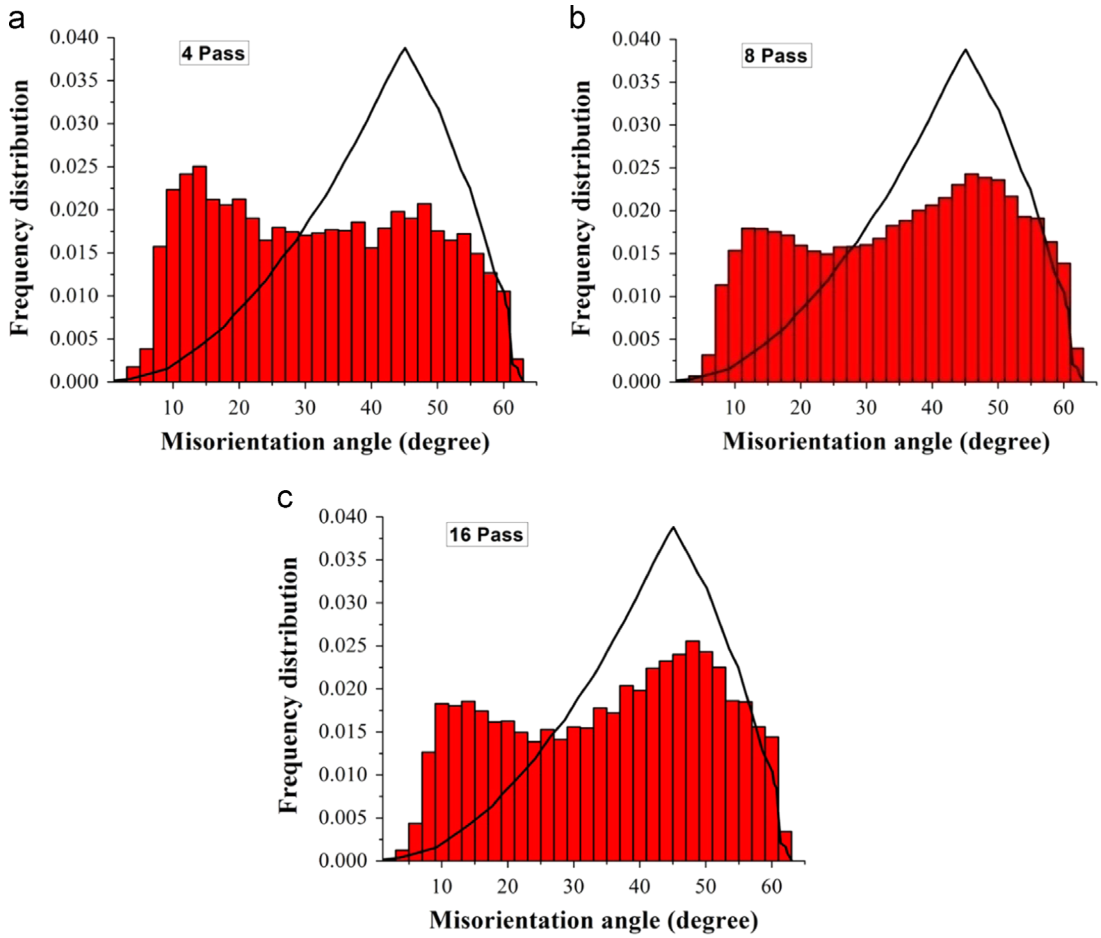

Fig. 7. Grain-to-grain misorientation distributions obtained by EBSD in comparison with the random Mackenzie distribution (solid line) for different samples after (a) 4 pass, (b) 8 pass and (c) 16 CEE pass.

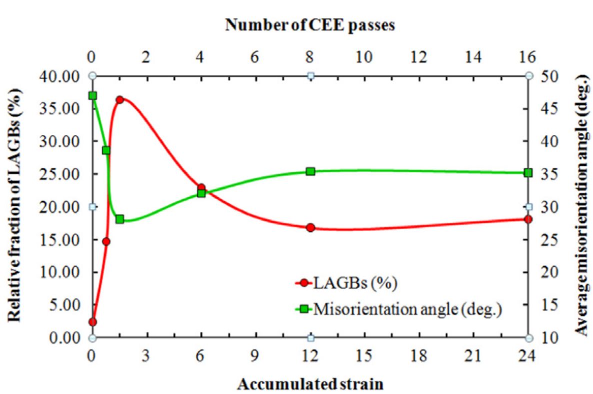

Fig. 8. Variation of the relative fraction of LAGBs and the average misorientation angle during CEE processing as a function of the von Mises equivalent accumulated strain.

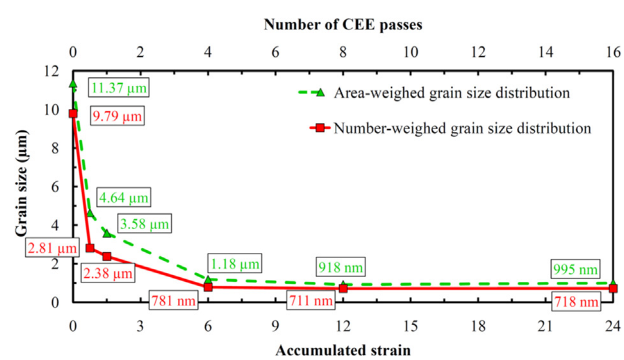

Fig. 9. Evolution of the average number and area-weighed grain sizes during CEE processing of pure copper.

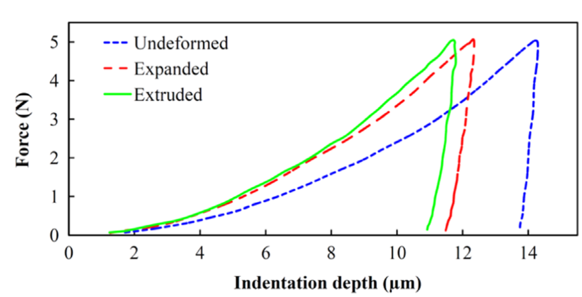

Fig. 10. Indentation load–displacement curves during the first CEE pass for different positions identified in Fig. 3.

indicates that the work hardening rate is smaller in the (b)-(c) stage (extrusion) than in the first (a)-(b) stage (expansion).

The evolution in microhardness and tensile properties as a function of strain are displayed in Fig. 11. Significant increase in the mechanical strength of the samples was observed after SPD processing by CEE. Both hardness and tensile properties (UTS and yield stress) show a maximum at similar accumulated strain values (at four CEE passes) and reach a steady state at strain values higher than $\varepsilon_{eq.} \sim 15$. Vorhauer et al. [33] have also found that there was no significant change in the microstructure of deformed OFHC copper samples beyond $\varepsilon_{eq.} \sim 16$ which is close to our result. These results are also coherent with the results published by Dalla Torre et al. [34] – also displayed in Fig. 11.

The tensile strength values in this study are also similar to others reported in [34–38]. Nevertheless, one difference is worth pointing out, which concerns the yield stress values. The yield stress is lower in CEE with respect to the data obtained in ECAP in [34] (see Fig. 11). The origin of this difference must be due to the difference in average grain size. In CEE the grain sizes are systematically larger than in ECAP – about twice [6] – which must result in lower yield stress in tension. It will be discussed in Section 4.6 below that the larger grain size is due to the cyclic nature of the CEE process. Note that the difference in texture between the CEE and ECAP processes cannot explain the differences in the yield stress because our Taylor factor simulations showed that the Taylor factors are nearly the same for a tensile testing of CEE or ECAP deformed polycrystal (3.14 and 3.16, respectively). Although the grain sizes are larger, thus the yield stress is smaller in a CEE processed copper sample with respect to ECAP, the difference is not much (about 10%). There are, however, several advantages of the CEE process with respect to ECAP. One of them is the simplicity of the test in CEE, and another is that there is no need to apply back pressure in the CEE process while in ECAP it is a must, in order to keep the geometry of the sample.

4.5. Texture analysis

The evolution of the crystallographic texture is shown in Fig. 12 in the form of inverse pole figures. The initial texture is relatively weak with mixed ⟨111⟩+⟨100⟩ fibers parallel to the extrusion direction (ED). After the first pass, the ⟨100⟩ decreases and the ⟨111⟩ strengthens significantly up to the fourth pass.

At the eighth pass, the ⟨00⟩ fiber component strengthens; it becomes quite strong and maintains its intensity up to pass no. 16. In previous works of extrusion and wire drawing of pure copper this component was attributed to dynamic recrystallization while the ⟨111⟩ fiber is known as the ultimate extrusion texture of FCC metals [39–42]. The strengthening of the ⟨100⟩ component leads to a decrease in flow stress because of its relatively low Taylor factor

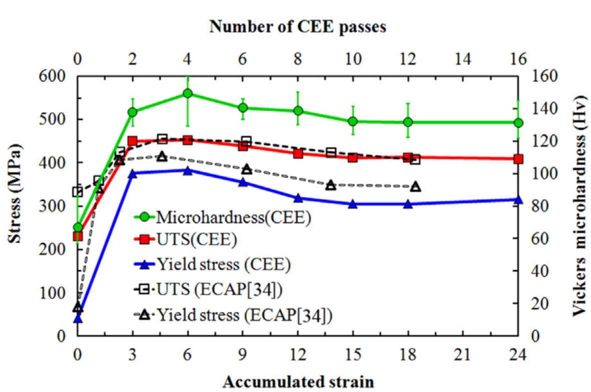

Fig. 11. Evolution of mechanical properties during CEE processing of pure copper in comparison with ECAP processing.

(2.5). Indeed, the flow stress is decreasing from pass no. 4. The reappearance of this component might be due to recrystallization which is also reported as a softening mechanism in ECAP-deformed copper samples at comparable strain values [34].

In order to elucidate the occurrence of dynamic recrystallization in the present CEE experiments, we have examined the grain orientation spread (GOS) around the three ideal fiber components using the EBSD IPF maps measured after the 16th pass. The average GOS was examined as a function of the deviation angle from the three ideal fiber positions, see Fig. 13a. Note that here the GOS of a grain was calculated as an average disorientation value with respect to the orientation of the center of gravity of the grain. This is not the usual Kernel average misorientation (KAM) – which is the average misorientation between all pixel points of the grain; our definition leads to smaller values (about twice smaller). However, we believe that the average misorientation with respect to a fix point in the grain is more representative to the real average lattice curvature of the grain. The average value of the GOS in the whole map was 2.2° which is above the value that would correspond to a recrystallized state (about 1° for the present GOS, or 2° in KAM [43,44]).

As can be seen in Fig. 13a, for the ⟨111⟩ fiber the GOS is nearly constant. However, for the ⟨100⟩ and ⟨110⟩ components there is a clear tendency of decreasing GOS as the ideal fiber position is approached. The relatively small GOS values for these two fibers could correspond – in principle – to the occurrence of recrystallization, however, the corresponding grain sizes are small, even smaller than the average grain size, see Fig. 13b. Therefore, it is clear that the origin of the ⟨100⟩ fiber cannot be DRX. Fig. 13c shows the EBSD-IPF map of the 16-pass sample illustrating the sharp texture of the material where the blue color represents the ⟨111⟩ fiber while the red one is the ⟨100⟩.

Another important feature of the texture evolution presented in Fig. 12 is the low intensity of the ⟨110⟩ component at any stage of deformation. The ⟨111⟩ and ⟨100⟩ double fiber components are characteristic for drawing/extrusion of pure copper [45–48]. However, during the expansion stage a ⟨110⟩ type fiber texture is expected which is characteristic for compression textures [49,50]. It is therefore expected that the second deformation stage of the CEE process – the extrusion – is the decisive stage for the final texture. This issue was experimentally examined on a sample stopped during pressing and extracted from the die during the first CEE pass (Fig. 3) and the results are illustrated in Fig. 14. A significant change in texture is observed within a single CEE pass (expansion and extrusion). The ⟨110⟩ texture in the expansion zone was very much reduced by the following extrusion stage giving rise to the ⟨111⟩ fiber (Fig. 14) and at a later stage also to the ⟨100⟩ (Fig. 12).

For understanding the observed texture evolution during one CEE pass, one has to take into account the cyclic nature of the CEE process. During each pass, the strain path begins with expansion, and then it is continued by extrusion, so the direction as well as the amount of strain are inverted and the grains recover their initial shape. In principle, complete inversion of the strain should lead to opposite texture evolution so the texture formed during

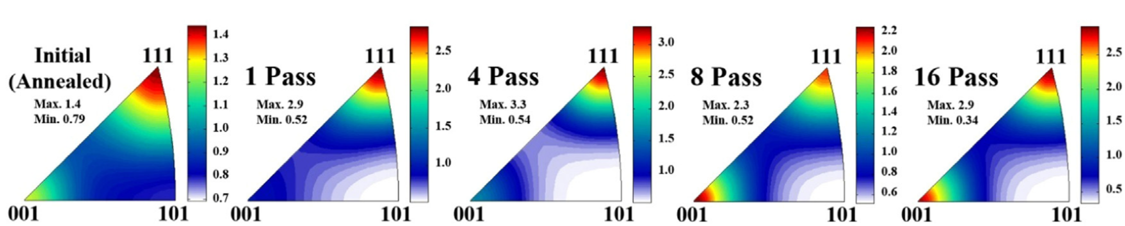

Fig. 12. The evolution of the crystallographic texture in inverse pole figures of the ED sample axis as a function of pass number during CEE processing of pure Cu, measured by X-ray. (For interpretation of the references to color in this figure legend, the reader is referred to the web version of this article.)

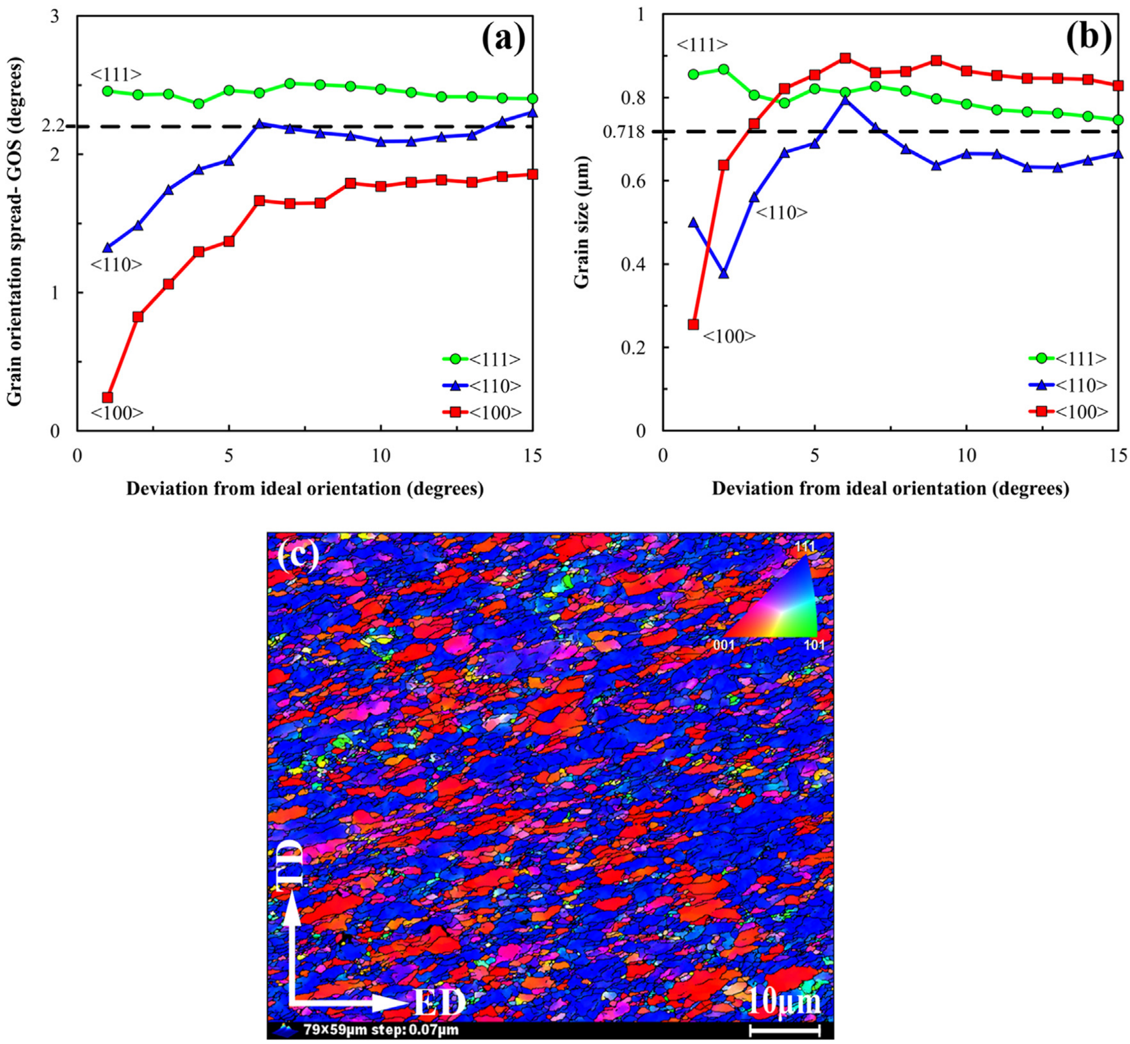

Fig. 13. (a) The average grain orientation spread and (b) the average grain size as a function of grain misorientation from the ideal fiber orientation for the 16 pass CEE deformed copper sample for the three ideal fibers: ⟨100⟩, ⟨110⟩ and ⟨111⟩. The horizontal broken line in (a) and (b) shows the average values on the whole map. (c) The EBSD-IPF map of the sample showing the projection of the ED direction with the color code defined in the insert.

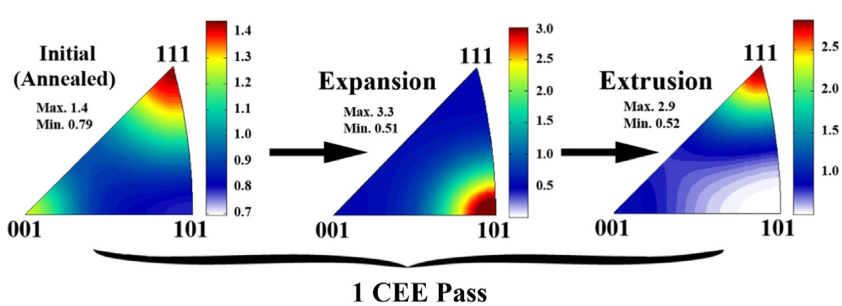

Fig. 14. The evolution of the crystallographic texture in inverse pole figures of the ED axis during 1-pass of CEE processing of pure copper. (For interpretation of the references to color in this figure legend, the reader is referred to the web version of this article.)

the first expansion stage should be dissolved during the second extrusion stage, and a texture similar to the initial one should appear. This is not what was observed experimentally; the ⟨111⟩ component becomes even stronger than it was in the initial state. The strain reversal textures were studied thoroughly for shear textures in Refs. [51,52]. The application of a sophisticated grain refinement model [53] in those works led to the conclusion that it is the grain refinement process which is responsible for the existence of the strain-reversal textures. The same mechanism is expected to be operational in the present CEE process because of the extensive grain fragmentation process documented above. Simulations of this phenomena are planned to explain the reversal textures in CEE processing by using the grain refinement model.

For a quantitative analysis of the textures, the volume fractions of the fiber textures from the X-ray texture measurements were calculated. In this regard, a special program was written to obtain the volume fractions from the X-ray experiments using the new JTEX software [27]. A large disorientation criterion from the ideal fiber axis was considered (up to 20°) in the calculations to count all grains that are in the vicinity of a fiber. The results are

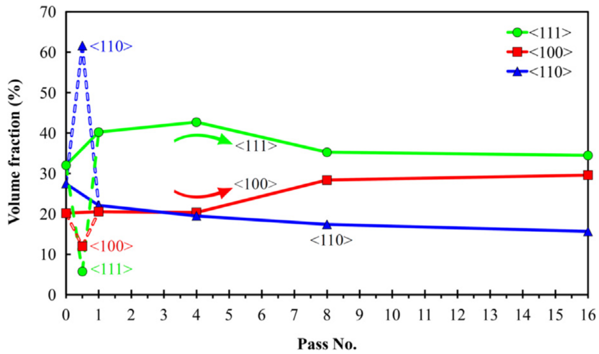

Fig. 15. Volume fractions of the fiber textures obtained from X-ray measurements as a function of pass-number in CEE processing of pure copper. Volume of individual grains is counted up to 20° disorientation.

presented in Fig. 15 which also includes the result for the texture measured at the middle of the first pass (i.e. between the expansion and extrusion zones).

As mentioned before, at mid-pass the texture becomes a strong ⟨110⟩ fiber (with a significantly higher volume fraction compared to the other two components) which transforms into a mixture of the three fibers in the extrusion stage. The evolution in volume fractions of the fiber textures (Fig. 15) can also explain the material softening after the 4th pass. It is seen in this figure that the ⟨111⟩ component has a peak at fourth pass then decreasing with further processing. At the same time, the ⟨100⟩ component increases after four passes. It should be noted that for an FCC structure with a 100% ⟨111⟩ component have the highest possible Taylor factor ($M_{\langle 111\rangle}=3.67$) compared to that of the ⟨100⟩ component ($M_{\langle 100\rangle}=2.5$). Therefore, simultaneous consideration of these facts can explain the softening observed in samples after the 4th CEE pass shown in Fig. 11.

It is also important to point out that the texture evolution shown within the first pass (Fig. 14) has to be repeated in every pass. We only show the detailed evolution of the texture in the first pass in Fig. 15, however, the variations shown by the broken lines for the three fibers are obviously taking place in each pass.

4.6. The limiting state

Finally, it is important to discuss the final state of the CEE processed pure copper. As can be seen in Fig. 9, the limiting steady state grain size is 718 nm. Comparing this value to other processes, it is significantly larger; in ECAE (in routes A or B), HPT, or HPTT (High Pressure Tube Twisting) the limiting grain size is about 270 nm [54]. The difference can be explained by the cyclic nature of the CEE process, namely, in each pass there are two stages of deformation, and during the second stage the strain is inverted. By inverting the strain path, a consequence is that the grain fragmentation process is less efficient. The reason for that has to be looked for in the population of the geometrically necessary dislocations which are responsible for the formation of new boundaries. During monotonic straining the GNDs are continuously pumped into the geometrically necessary boundaries (GNBs) in which the disorientation is increasing. However, when the strain is inverted, many of the GNDs move in the opposite direction, so there is a decrease in GND density in the GNBs. The consequence is that the boundary angles stop increasing, they might even decrease. The result of this process is that the speed of the grain fragmentation process is reduced so the final limiting grain size becomes larger. This difference was examined above in Section 4.4 and explains the slightly lower yield stress (about 10% lower) in the CEE processed samples with respect to ECAP processing.

5. Conclusions

The present study was devoted to investigation of microstructure, texture and mechanical properties evolution and their relationship in commercial pure copper samples subjected up to 16 passes in cyclic expansion–extrusion (CEE) process. From the results obtained, the following major conclusions can be drawn:

1. The CEE SPD technique is a suitable process to refine the microstructure of copper while keeping the sample dimension constant. The obtained mechanical characteristics approach those obtained by other SPD techniques.
2. A steady state is reached already after eight CEE passes with a characteristic grain size and crystallographic texture. The steady state grain size is about twice larger than in ECAP due to the cyclic strain reversal nature of the deformation process.
3. There is a significant evolution in the crystallographic texture within each pass and also after the passes as a function of pass number. Up to the 4th pass, the ⟨111⟩ fiber component is strengthening at the expense of the ⟨110⟩ fiber. Between the 4th and 8th passes the ⟨111⟩ weakens and the ⟨100⟩ strengthens. The lowering of the yield stress from the 8th pass in the steady state stage can be related to the relative proportion of the texture components.
4. A relatively small grain orientation spread together with a smaller grain size was observed in the vicinity of the ⟨100⟩ and ⟨110⟩ ideal fibers confirming the absence of a dynamic recrystallization process for these components.

Acknowledgments

Financial support by the Research Council Office of Shiraz University through Grant number 92-GR-ENG-15 is appreciated. N. Pardis acknowledges the Tallinn University of Technology for receiving him on sabbatical leave. This work was also supported by the French State through the program "Investment in the Future" operated by the National Research Agency (ANR) and referenced by ANR-11-LABX-0008-01 (LabEx DAMAS). CFG acknowledges the ARC DECRA Scheme for the financial supports DE 130100274. Part of this research was supported by the European Social Fund in the framework of the DoRa program, carried out by Archimedes foundation.

References

[1] A.P. Zhilyaev, T.G. Langdon, Prog. Mater. Sci. 53 (2008) 893–979.
[2] V.M. Segal, Mater. Sci. Eng. A 197 (1995) 157–164.
[3] M. Furukawa, Z. Horita, M. Nemoto, T.G. Langdon, J. Mater. Sci. 36 (2001) 2835–2843.
[4] R.Z. Valiev, T.G. Langdon, Prog. Mater. Sci. 51 (2006) 881–981.
[5] T.G. Langdon, J. Mater. Sci. 42 (2007) 3388–3397.
[6] L.S. Toth, C.F. Gu, Mater. Charact. 92 (2014) 1–14.
[7] Y.T. Zhu, T.G. Langdon, J. Miner. Met. Mater. Soc. 56 (2004) 58–63.
[8] R.Z. Valiev, T.G. Langdon, Metall. Mater. Trans. A 42 (2011) 2942–2951.
[9] R.Z. Valiev, R.K. Islamgaliev, I.V. Alexandrov, Prog. Mater. Sci. 45 (2000) 103–189.
[10] Y. Estrin, A. Vinogradov, Acta Mater. 61 (2013) 782–817.
[11] A. Azushima, R. Kopp, A. Korhonen, D.Y. Yang, F. Micari, G.D. Lahoti, P. Groche, J. Yanagimoto, N. Tsuji, A. Rosochowski, A. Yanagida, CIRP Ann. Manuf. Technol. 57 (2008) 716–735.
[12] N. Pardis, R. Ebrahimi, Mater. Sci. Eng. A 527 (2009) 355–360.
[13] Ch.P. Wang, F.G. Li, L. Wang, H.J. Qiao, Sci. China Technol. Sci. 55 (2012) 2377–2390.
[14] N. Pardis, B. Talebanpour, R. Ebrahimi, S. Zomorodian, Mater. Sci. Eng. A 528 (2011) 7537–7540.
[15] N. Pardis, C. Chen, M. Shahbaz, R. Ebrahimi, L.S. Toth, Mater. Sci. Eng. A 613 (2014) 357–364.
[16] J. Richert, M. Richert, Aluminium 62 (1986) 604–607.
[17] J. Pluta, Sborník vědeckých prací Vysoké školy báňské (2007) 107–110.

[18] J. Richert, M. Richert, M. Mroczkowski, Int. J. Mater. Form. 1 (2008) 479–482.
[19] M. Richert, Solid State Phenom. 114 (2006) 19–28.
[20] H. Lianxi, L. Yuping, W. Erde, Y. Yang, Mater. Sci. Eng. A 422 (2006) 327–332.
[21] I. Balasundar, K.R. Ravi, T. Raghu, Mater. Sci. Eng. A 583 (2013) 114–122.
[22] J. Lin, Q. Wang, L. Peng, H.J. Roven, J. Mater. Sci. 43 (2008) 6920–6924.
[23] I. Balasundar, T. Raghu, Int. J. Mater. Form. 6 (2013) 289–301.
[24] K. Mills, J.R. Davis, sixth printing, Metals Handbook, vol. 9, ASM International, Materials Park, OH, 1995.
[25] B. Beausir, Software for orientation image mapping, http://www.lem3.fr/beausir/Benoit/#downloads.
[26] L.S. Toth, B. Beausir, C.F. Gu, Y. Estrin, N. Scheerbaum, C.H.J. Davies, Acta Mater. 58 (2010) 6706–6716.
[27] J.-J. Fundenberger, B. Beausir, Université de Lorraine – Metz, 2015, JTEX – Software for Texture Analysis, ⟨http://jtex-software.eu/⟩.
[28] W. Hosford, R. Caddell, Metal Forming Mechanics and Metallurgy, third ed., Cambridge University Press, Cambridge, 2007.
[29] Abaqus/Explicit User's Manual, Version 6.3, Hibbitt, Karlsson & Sorensen, Inc., USA, 2002.
[30] N.Q. Chinh, G. Horvath, Z. Horita, T.G. Langdon, Acta Mater. 52 (2004) 3555–3563.
[31] J.K. Mackenzie, M.J. Thomson, Biometrika 44 (1957) 205–210.
[32] J.K. Mackenzie, Biometrika 45 (1958) 229–240.
[33] A. Vorhauer, S. Scheriau, R. Pippan, Metall. Mater. Trans. A39 (2008) 908–918.
[34] F.D. Torre, R. Lapovok, J. Sandlin, P.F. Thomson, C.H.J. Davies, E.V. Pereloma, Acta Mater. 52 (2004) 4819–4832.
[35] O.F. Higuera-Cobos, J.M Cabrera, Mater. Sci. Eng. A 571 (2013) 103–114.
[36] A. Mishra, B.K. Kad, F. Gregori, M.A. Meyers, Acta Mater. 55 (2007) 13–28.
[37] G. Purcek, O. Saray, M.I. Nagimov, A.A. Nazarov, I.M. Safarov, V.N. Danilenko, O. R. Valiakhmetov, R.R. Mulyukov, Philos. Mag. 92 (2012) 690–704.
[38] F.H. Dalla Torre, A.A. Gazder, E.V. Pereloma, C.H.J. Davies, J. Mater. Sci. 42 (2007) 1622–1637.
[39] D.N. Lee, Scr. Metall. Mater. 32 (1995) 1689–1694.
[40] R.A. Vandermeer, C.J. McHargue, Trans. Metall. Soc. AIME 230 (1964) 667–675.
[41] W.R. Hibbard, Trans. AIME 77 (1950) 581–585.
[42] H. Ahlborn, G. Wassermann, Z. Metall. 54 (1963) 1–6.
[43] S.I. Wright, M.M. Nowell, D.P. Field, Microsc. Microanal. 17 (2011) 316–329.
[44] A. Ayad, F. Wagner, N. Rouag, A.D. Rollett, Comput. Mater. Sci. 68 (2013) 189–197.
[45] I.L. Dillamore, W.T. Roberts, Metall. Rev. 10 (1965) 271–380.
[46] H. Hu, Texture 1 (1974) 233–258.
[47] D.R. Waryoba, P.N. Kalu, Extraction and Processing Division (EPD) Congress, 2005, pp. 247–258.
[48] P.N. Kalu, D.R. Waryoba, Mater. Sci. Forum 550 (2007) 509–514.
[49] W. Gambin, Plasticity and Texture, Kluwer Academic Publishers, Netherlands, 2001.
[50] A.M. Wusatowska-Sarnek, H. Miura, T. Sakai, Mater. Sci. Eng. A 323 (2002) 177–186.
[51] C.F. Gu, L.S. Toth, C.H.J. Davies, Scr. Mater. 65 (2011) 167–170.
[52] C.F. Gu, L.S. Toth, Acta Mater. 59 (2011) 5749–5757.
[53] L.S. Toth, Y. Estrin, R. Lapovok, C.F. Gu, Acta Mater. 58 (2010) 1782–1794.
[54] A. Pougis, L.S. Toth, J.J. Fundenberger, A. Borbely, Scr. Mater. 72–73 (2014) 59–62.